UDC 539.4

U-SANS Analysis of As-Sintered and PEC-Treated NiTi SMA Produced by Metal Injection Moulding

A. Giuliani,[a] V. Calbucci,[a] F. Fiori,[a] P. Imgrund,[b] and A. I. Babutskii[c]

[a] Marche Polytechnic University, Ancona, Italy

[b] Fraunhofer Institute of Manufacturing and Advanced Materials, Bremen, Germany

[c] Pisarenko Institute of Problems of Strength, National Academy of Sciences of Ukraine, Kiev, Ukraine

УДК 539.4

Анализ исходного и обработанного импульсным электрическим током никель-титанового сплава, полученного методом инжекции, при использовании ультрамалоуглового рассеивания нейтронов

А. Джулиани[а], В. Калбуччи[а], Ф. Фиори[а], Ф. Имгрунд[б], А. И. Бабуцкий[в]

[а] Политехнический университет области Марке, Анкона, Италия

[б] Фраунгоферский институт промышленности и современных материалов, Бремен, Германия

[в] Институт проблем прочности им. Г. С. Писаренко НАН Украины, Киев, Украина

С использованием метода, основанного на ультрамалоугловом рассеивании нейтронов, выполнен анализ размеров пор диаметром 100 нм ... 25 мкм в полученных инжекционной формовкой образцах из никель-титанового сплава (с памятью формы) до и после обработки импульсным электрическим током. При обработке образцов поры диаметром меньше 4 мкм коалесцируют, а поры диаметром больше 4 мкм уменьшаются в размерах.

Ключевые слова: метод ультрамалоуглового рассеивания нейтронов, инжекционная формовка, импульсный электрический ток.

Introduction. The study of the electromagnetic field effects on dislocations and other defects involved in the deformation process of polycrystalline solids is still a challenge in material science. In fact, according to the review of the present work authors, the influence of specific electric fields was clarified just in a few conventional materials like steels, cast iron and the principal aluminum and titanium alloys [1]. On the other hand, it is assessed that an electric field offers an additional parameter in metal processing with the potential of increasing the efficiency and effectiveness of the process, improving the final resulting thermomechanical properties.

For instance, high density (10^3–10^6 A/cm^2) electropulsing influences the flow stress of metals at 78–300 K during their tensile deformation, significantly reducing the flow stress (or increasing the strain rate) [2–5].

The effects of an external electric field (surface charge) on the superplastic deformation of the 7475 Al alloy were investigated and it was found that the field produced the following effects [6–10]: (a) reduced the flow stress by 10–20%, (b) slightly increased the strain rate hardening exponent $m = \partial \ln \sigma / \partial \ln \varepsilon$, (c) slightly increased the width of the dispersoid-free zone at the grain boundaries. In the case of 7475 Al alloy, the field also changed the chemical composition and enhanced the formation of whiskers; therefore: (d) retarding grain growth and (e) significantly reducing cavitation.

The effects of electric fields were also tested during the superplastic deformation of 3Y-TZP. Even in this case, the electric field reduced the flow stress and increased the elongation. Along with its effect on the stress–strain curve, the field retarded grain growth and cavitation [11].

For the first time in the present work, pulse electric current (PEC) treatment was applied to NiTi SMA specimens produced by metal injection moulding (MIM).

Ultra-small angle neutron scattering (U-SANS) analysis was performed on NiTi specimens in order to verify if defect (pore) size varies after the PEC treatment in the dimensional range between 100 nm and 25 μm. U-SANS technique is in fact a suitable characterization method in order to get such answer in this range.

1. **Materials and Methods**.

1.1. ***NiTi Specimens Preparation by MIM***. MIM was first used for NiTi processing by Bram et al. [12]. In the present process, prealloyed NiTi powder with a powder particle size $d_{\varnothing} = 11.3$ μm and an atomic ratio of 50.7% Ni–49.3% Ti was mixed with an organic binder of waxes and polymers to obtain the feedstock. Specimens were moulded as in conventional injection moulding. The binder was then retracted from the part and sintered at 1250°C under high vacuum (10^{-4} mbar).

Density measurements by the Archimedes method showed that a density of 91–94% of theoretical density was obtained after sintering. The process and some of the obtained moulded parts are depicted in Fig. 1.

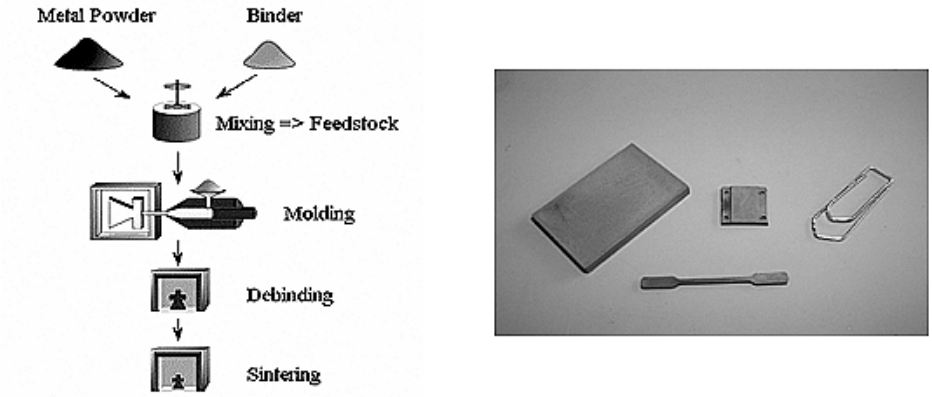

Fig. 1. MIM process (left) and NiTi green parts (right).

1.2. ***PEC Treatment of NiTi Specimens***. PEC treatment was fulfilled using a pulse electric current generator consisting of a high voltage power supplier, capacitor banks and discharge switch. Registration of the pulse electric current

parameters was realized using Rogovsky coil, high frequency A/D converter and PC where data were stored and processed. The treatment was carried out by direct current passage through the NiTi specimen. Three short sequential pulses of the electric current with the maximum amplitude of 52 kA – 56 kA – 52 kA were passed through the specimen, here the specimen sectional area was near 80 mm^2.

2. **Experimental Methods**.

2.1. ***Preliminary Characterization by Scanning Electron Microscopy and Energy Dispersive X-ray Analysis***. As-sintered NiTi specimens were characterized by means of scanning electron microscopy (SEM) and energy dispersive X-ray (EDX) analyses for a preliminary determination of pore size, Ni–Ti ratio and phase compositions. The microstructure, as revealed by SEM, is shown in Fig. 2.

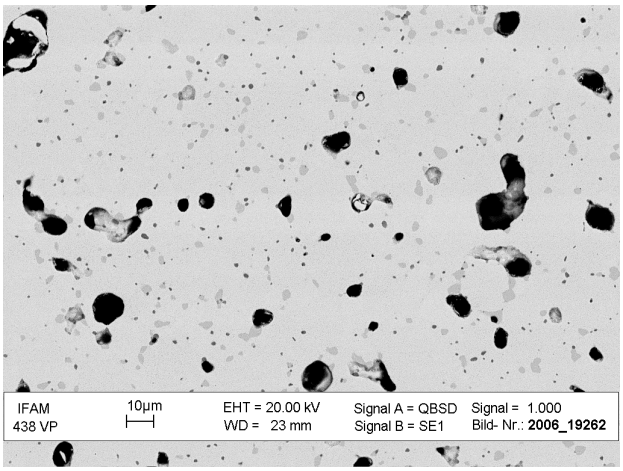

Fig. 2. SEM micrograph of NiTi after MIM and sintering at 1250℃ under high vacuum.

Concerning composition, two different phases were detected by EDX analyses. The light grey matrix phase was found to be NiTi: the atomic ratio detected was 50.3 Ni–49.7 Ti, which was in good accordance with the base material composition. The slightly darker phase revealed a Ni/Ti ratio of 33/67, indicating the presence, after sintering, of a very low amount of $NiTi_2$ secondary phase. Figure 2 shows such multi-phase microstructure along with some irregular porosity. In fact, together with large irregularly shaped pores, different fine, spherical pores were detected, demonstrating the necessity to investigate the PEC treatment effects on NiTi by U-SANS, such technique being sensitive at a scale range comparable with the latter pore dimensional group.

2.2. ***Characterization by the U-SANS***. U-SANS analysis was performed at the double crystal diffractometer (DCD) instrument at the Geesthacht Neutron Facility (Geesthacht, Germany) on NiTi specimens produced by MIM before and after the PEC treatment. The DCD, in the chosen set-up, was equipped with triple-bounce channel-cut perfect Si crystals [13]. Using the (111) reflection, the full width at half-maximum (FWHM) of the rocking curve (RC) is about $2.6 \cdot 10^{-4}$ nm^{-1} at a wavelength of $\lambda = 0.44$ nm.

When compared with single-bounce crystals, the instrumental background at a scattering vector $Q = 10^{-3}$ nm^{-1} is decreased by two orders of magnitude: this

leads to enormous progress involving the possibility to detect small volume fractions of inhomogeneities in the size range from 100 nm up to about 25 μm [14].

Because of this, DCD was selected and used in the present work to analyze shape, size distribution and volume fraction of pores and the effects of the PEC treatment on them.

Pore size distribution $N(R)$ shall be defined in the radius interval $[R_{\min}, R_{\max}]$: it can be written as a linear combination of m basic size distributions $n_i(R)$ with coefficients x_i:

$$N(R) = \sum_{i=1}^{m} x_i n_i(R). \tag{1}$$

Cubic B-splines are chosen for the basic size distributions $n_i(R)$. With such a set of basic functions, an arbitrary smooth function can be approximated [15, 16].

We numerically treated the data obtained on both PEC-treated and untreated specimens with a model based on two phases coexistence: the NiTi phase and another phase corresponding to pores. This model is called *two-phase model* and is based on the assumption of the presence of pores with a size distribution $N(R)$, embedded in a homogeneous matrix (polidispersion). The Master equation of such model is the following [17, 18]:

$$\frac{d\Sigma}{d\Omega} = (\Delta\rho)^2 \int_0^\infty N(R) V^2(R) \left| F(QR) \right|^2 dR, \tag{2}$$

where $d\Sigma/d\Omega$ is the macroscopic cross section of pores (the measured quantity), $(\Delta\rho)^2$ is the nuclear contrast between the pores and the matrix, $V(R)$ is the pore volume, and $F(QR)$ is the pore form factor. In our case, on the basis of preliminary SEM analysis (Sec. 2.1), we considered a sphere-like form factor, corresponding pores approximately spherical in shape.

Under these conditions it is also possible to estimate pore *volume fraction* f by means of the following equation:

$$f = \int N(R) V(R) dr. \tag{3}$$

An estimate of the pore size can also be obtained by means of the Guinier approximation. As far as this is valid, that is for $QR_G \le 1.5$ (approximately), Eq. (2) can be written as

$$\frac{d\Sigma}{d\Omega} \approx (\Delta\rho)^2 n V^2 \exp\left(-\frac{Q^2 R_G^2}{3} \right), \tag{4}$$

where n is the number density of pores and R_G is the Guinier radius. For spherical pores with radius R, $R_G = \sqrt{3/5}R$; in the case of polydispersion, R_G depends on the size distribution:

$$R_G^2 = \frac{\int_0^\infty R^8 N(R) dR}{\int_0^\infty R^6 N(R) dR}, \tag{5}$$

R_G is usually determined by the slope, at low Q values, of the linear plot $\ln(d\Sigma/d\Omega)$ vs. Q^2. Anyway an alternative (and even more direct) method is by plotting $Q^2(d\Sigma/d\Omega)$ vs. Q. In fact, from Eq. (4), it is easy to verify that this function has a maximum for $Q = \sqrt{3}/R_G$.

3. **Results**. The $Q^2(d\Sigma/d\Omega)$ vs. Q plots for the untreated and PEC-treated specimens are shown in Fig. 3. In the untreated profile, two peaks corresponding to two pore families are detected, one with $R_G = 2.37$ μm and the other with $R_G = 8.75$ μm. In the PEC-treated case, only the peak corresponding to the biggest family is clearly visible, with a Guinier radius smaller than the one for the untreated specimen ($R_G = 5.83$ μm); on the contrary, the peak corresponding to the smaller family is not detectable.

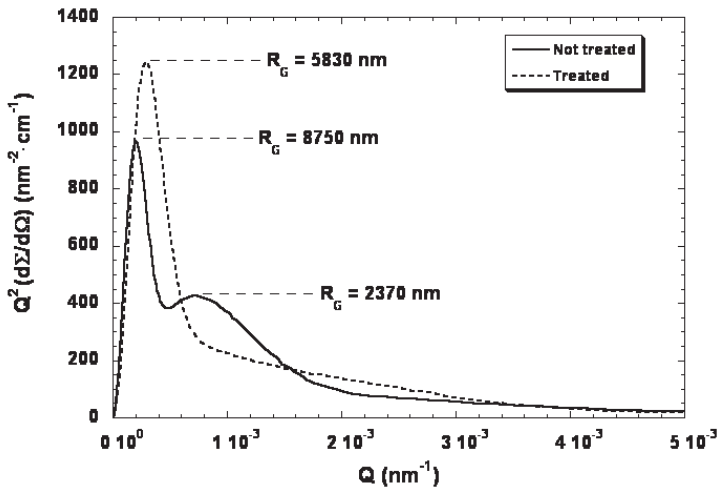

Fig. 3. $Q^2(d\Sigma/d\Omega)$ vs. Q plots for the PEC-treated (dot-line) and the untreated (solid line) specimens.

In Fig. 4 the DCD scattering curves from the PEC-treated (dotted line) and the untreated (solid line) NiTi specimens are shown, superimposed to the best fit curve obtained by writing $N(R)$ as a linear combination of cubic B-spline functions $\beta_i(R)$:

$$N(R) = \sum_{i=1}^{N_s} c_i \beta_i(R) \rightarrow \frac{d\Sigma}{d\Omega} = (\Delta\rho)^2 \sum_{i=1}^{N_s} c_i \int_0^\infty \beta_i(R) V^2(R) \left| F(QR) \right|^2 dR. \tag{6}$$

The coefficients c_i are the parameters optimized by the least-square fit and resulting in the pore size distribution $N(R)$ shown in Fig. 5.

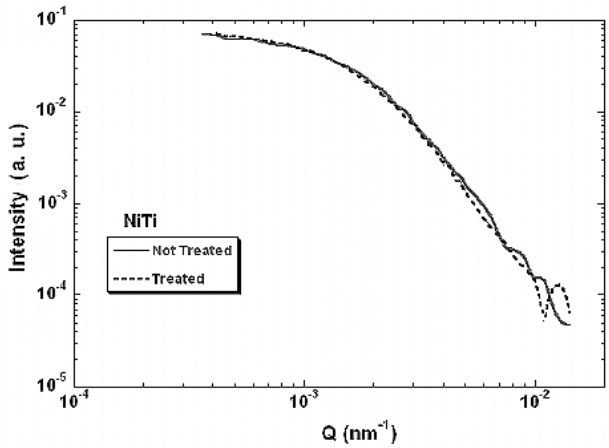

Fig. 4. DCD scattering curves for the PEC-treated (dot-line) and the untreated (solid line) specimens.

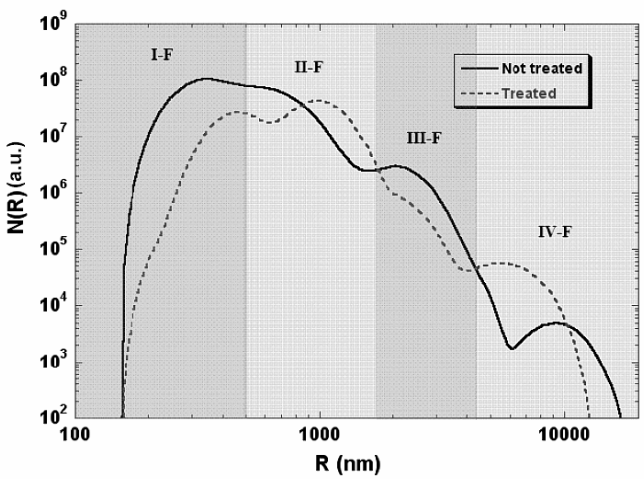

Fig. 5. Pore size distribution in the PEC-treated specimens (dot-curve) and in the untreated ones (solid curve).

The $N(R)$ size distribution is four-modal (4 peaks in each curve) (Fig. 5). In the untreated specimen there is a first big family of pores (*I-F*) with a main pore radius slightly bigger than 400 nm, another family (*II-F*) with average radius close to 800 nm, a third group (*III-F*) with a radius close to 2.5 μm and the last family (*IV-F*) with a radius close to 10 μm.

It is visible from the results presented in Fig. 5 that after PEC treatment the redistribution of the pores numbers took place: the total pores' number in the former *I-F* and *III-F* families was reduced; in the *II-F* family, the pores' number with smaller dimension was reduced and the pores' number with bigger dimension was increased; and vice versa for the last *IV-F* family, the share of pores with smaller dimension was increased against the reduction of the big pores' number.

The volume fractions for each pore family can be calculated as the integral of the curves $N(R)V(R)$ vs. R, where $N(R)$ is the size distribution, $V(R)$ is the volume of the pore, and R is its radius, i.e., applying (2) and (3) and extrapolating the results shown in Fig. 6.

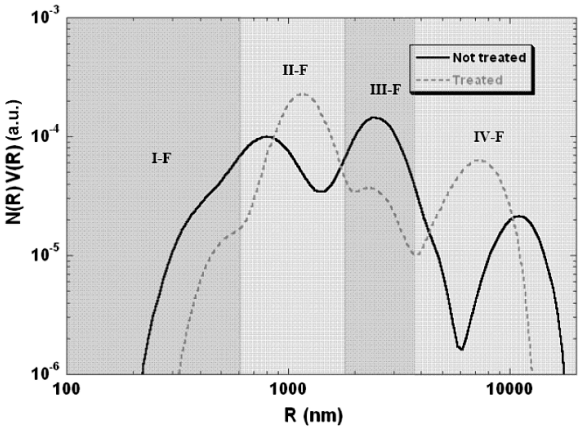

Fig. 6. Pore volume fraction (integrated area) in the PEC-treated specimens (dotted curve) and in the untreated ones (solid curve).

In the untreated specimen (solid-line) the *I-F* (R close to 400 nm) exhibits a small volume fraction. This is justified by very small volume of such pores. The second family, with the average radius close to 800 μm has a quite high volume fraction close to 2/3 of the third group (that one with R close to 2.5 μm). The fourth family with an average pore radius close to 10 μm has a very small volume fraction: this is due to the almost negligible amount of pores of such size, as it is detectable by SEM (Sec. 2.1). After the PEC treatment the volume fraction of the first family of pores is reduced, the volume fraction of the second family significantly increased and that of the third family significantly reduced. In contrast to the other three families, the trend of the last group (with a radius close to 10 μm before PEC treatment), after the treatment exhibit at the meantime an increasing of its volume fraction and significant reduction of its pore radius from 10 μm to less than 8 μm. These results (at least for what concerns the *III-F* and the *IV-F*) are in good agreement with the ones previously obtained by the Guinier approximation.

Analysis of the results obtained shows substantial redistribution of pore numbers depending of their sizes due to PEC treatment. This is takes place via coalescence of pores and reduction of their sizes. In addition, an annihilation of small pores is possible. The reason of these processes can be a vacancy movement generated by the pores under passage of electric current through the material [19]. At least two mechanisms of stimulation of vacancy generation exist: the first one is related to entrainment of the vacancies by conductivity electrons and the second one is related to nonhomogeneity of temperature distribution in the material caused by inhomogeneous Joule heat release in the defects of material structure (e.g., in pores). Generated temperature gradients cause local thermal stresses contributing pores coalescence and emission of vacancy-type dislocation loops. It causes the reduction of pore sizes and, as extreme case, results in pores' annihilation.

Conclusions. U-SANS was successfully applied for microstructural analysis of NiTi shape memory alloys submitted to PEC treatment. In particular, quantitative information about structure in the size range between 100 nm and a few tens of μm were obtained. This technique gave us a possibility to investigate parameters such as cavity density and dimensions, before and after the PEC treatment.

The phase morphology of the material (presence of pores) before and after PEC treatment has yielded data required for the optimization of the processing routes.

The results described in the previous chapter corroborate that, while pores with diameter smaller than 4 μm undergo coalescence phenomena after the PEC treatment, with a reduction of pores number but a crucial increase of their dimensions, in pores with diameter bigger than 4 μm the PEC treatment causes pore size reduction.

Redistribution of pores numbers demands a more precise definition of physical mechanisms through further microstructure investigations.

Acknowledgments. The authors acknowledge the help of Dr. K. Pranzas for the technical support during the U-SANS experiment at GKSS. This research has been supported by the European Commission under the 6th Framework Programme through the Key Action: Strengthening the European Research Area, Research Infrastructures. Contract No.: RII3-CT-2003-505925 (NMI3).

This work was also supported by the EU Network of Excellence project Knowledge-based Multicomponent Materials for Durable and Safe Performance (KMM-NoE) under the contract No. NMP3-CT-2004-502243.

Р е з ю м е

Із використанням методу, що базується на ультрамалокутовому розсіянні нейтронів, проаналізовано розміри пор діаметром 100 нм...25 мкм в отриманих інжекційним формуванням зразках нікель-титанового сплаву (із пам'яттю форми) до і після обробки імпульсним електричним струмом. При обробці зразків пори діаметром, який менше за 4 мкм, зливаються, а більше за 4 мкм, зменшуються в розмірах.

1. H. Conrad, "Some effects of an electric field on the plastic deformation of metals and ceramics," *Mat. Res. Innovat.*, **2**, 1–8 (1998).
2. A. F. Sprecher, S. L. Mannan, and H. Conrad, "On the mechanisms for the elector plastic effect in metals," *Acta Metall.*, **34**, 1145–1162 (1986).
3. H. Conrad and A. F. Sprecher, "The electroplastic effect in metals," in: F. R. N. Nabarro (Ed.), *Dislocations in Solids*, Ch. 43. Elsevier Science Publ. BV (1989), p. 499.
4. W. Cao, A. F. Sprecher, and H. Conrad, "The electroplastic effect in niobium in high temperature niobium alloys," in: J. J. Stephens and I. Ahmed (Eds.), *High Temperature Niobium Alloys*, TMS, Warrendale, PA (1991), p. 27.
5. W. Cao and H. Conrad, "Effect of stacking fault-energy and temperature on the electroplastic effect in FCC metals," in: S. Chu et al. (Eds.), *Micromechanics of Advanced Materials*, TMS, Warrendale, PA (1995), p. 225.
6. W. Cao, X. Lu, A. F. Sprecher, and H. Conrad, "Superplastic behaviour and microstructure of 7475 Al deformed in an external electric field," in: T. McNelly and H. Heikkenean (Eds.), *Superplasticity in Aerospace*, II, TMS, Warrendale, PA (1990), p. 269.

7. W. Cao, X. Lu, A. F. Sprecher, and H. Conrad, "Superplastic deformation behavior of 7475 aluminum alloy in an electric field," *Mater. Sci. Eng.*, **A138**, 247 (1990).
8. H. Conrad, W. Cao, X. Lu, and A. F. Sprecher, "Effect of electric field on cavitation in superplastic aluminum alloy 7475," *Mater. Sci. Eng.*, **A138**, 247–258 (1991).
9. X. Lu, W. Cao, A. F. Sprecher, and H. Conrad, "Influence of an external electric field on the microstructure of superplastically deformed 7475 Al," *J. Mater. Sci.*, **27**, 2243–2250 (1992).
10. W. Cao, X. Lu, and H. Conrad, "Whisker formation and the mechanism of superplastic deformation," *Acta Mater.*, **44**, 697–706 (1996).
11. S. L. Hwang and I. W. Chen, "Grain size control of tetragonal zirconia polycrystals using space charge concept," *J. Amer. Ceram. Soc.*, **73**, 3269 (1990).
12. M. Bram, A. Ahmad-Khanlou, A. Heckmann, et al., "Powder metallurgical fabrication processes for NiTi shape memory alloy parts," *Mat. Sci. Eng.*, **A337**, 254 (2002).
13. D. Bellmann, M. Klatt, R. Kampmann, and R. Wagner, "Improvement of the double crystal diffractometer at the Geesthacht Neutron Facility (GeNF) by means of perfect channel-cut silicon crystals," *Physica B*, **241-243**, 71–73 (1998).
14. P. Staron and D. Bellmann, "Analysis of neutron double-crystal diffractometer scattering curves including multiple scattering," *J. Appl. Cryst.*, **35**, 75–81 (2002).
15. O. Glatter, "A new method for the evaluation of small-angle scattering data," *Ibid*, **10**, 415–421 (1977).
16. O. Glatter, "Determination of particle-size distribution functions from small-angle scattering data by means of the indirect transformation method," *Ibid*, **13**, 7–11 (1980).
17. A. Guinier and G. Fournet, *Small-Angle Scattering of X-Rays*, Wiley, New York (1955).
18. G. Kostorz, *Treatise on Materials Science and Technology*, in: G. Kostorz and H. Herman (Eds.), *Neutron Scattering*, Vol. 15, Academic Press, New York (1979), p. 227.
19. S. V. Venginskaya and Yu. V. Kornyushin, "On a possibility of curing of extended defects by carry of vacancies used stimulation by an electric current," *Metallofiz. Nov. Tekhnol.*, Issue 61, 72–75 (1975).

Received 22. 04. 2009